Numerical Simulation of Non-Newtonian Blood Flow through a Tapered Stenosed Artery using the Cross Model

IOP Conf. Series: Materials Science and Engineering **864** (2020) 012200 doi:10.1088/1757-899X/864/1/012200

Numerical Simulation of Non-Newtonian Blood Flow through a Tapered Stenosed Artery using the Cross Model

T Majekodunmi Joshua[1], Anwar K[1] and Abdullah N[1]

[1]Institute of Engineering Mathematics, University Malaysia Perlis, Malaysia

E-mail: majekjoe1@gmail.com

Abstract: A Non-Newtonian model is used to examine the effect of tapering on the flow of blood along a stenosed artery which is caused by the pulsating nature the heart. The constitutive equation of the Cross model is used to capture the rheology of the streaming blood which accounts for the shear thinning behaviour of blood. The flow is considered to be laminar, incompressible, and axisymmetric. The finite- difference scheme was adopted to solve the non-linear equations describing the fluid motion in an unsteady two-dimensional case. The computation is presented in terms of the axial and radial velocities, volumetric flow rate, resistance to flow and the wall shear stress. The result from the numerical simulation clearly indicates that vessel tapering has considerable effect on the flow pattern of blood: as the tapering angle increases the flow rate and the axial velocity increases proportionately while the radial velocity, wall shear stress decreases and resistance to flow.

1. Introduction

The most important transport medium in the human body is the Blood. The free flow of blood is often challenged by Stenosis which is formed by the accumulation of fatty materials (called plaque) in the lining of the arterial wall which results in inadequate supply of oxygen and blood to the surrounding tissues and cardiac muscles. Stenosis has drawn the interest of scientists from various fields into the study of its clinical manifestation. Despite these attempts, its pathophysiology still remains elusive and obscure due to numerous associated risk factors. This arterial obstruction usually results in the development of several cardiovascular diseases which include angina, stoke, cardiac arrest (heart attack) and sometimes death [1].

A number of experimental and theoretical studies to investigate the flow of blood along the arteries treated blood as a Newtonian fluid [2]. These attempts were made with an intent of showing the effect of stenosis geometry on flow patterns.

The shear thinning, viscoelastic, thixotropic and suspension nature of blood shows that blood predominantly exhibits non-Newtonian properties. The Newtonian assumption does not account for these behaviours of blood hence, it is regarded to be inadequate. [3]. Rabby, Razzak, & Molla [4] compared the Newtonian and non- Newtonian case assuming the flow of blood to be pulsatile observed that the non-Newtonian assumption gave a better description of the flow condition.

The rheological properties of blood are usually modeled by higher constitutive equations over a shear-rate range and used as a vital tool for meaningful analysis and interpretation of blood flow. Several viscosity models have been employed to unravel the complexity of the non-Newtonian blood [5]. These studies assume the flow to be unsteady. Shupti, Molla, & Mia [6] examined the blood flow

response using four non-Newtonian models: Carreau, Cross, modified Casson and Quemada and noted that the pressure distribution is largely affected by increase in the Reynolds number. [7] found out that both wall shear stress and the flow resistance increased that such increase is obvious for converging artery in Hershel-Bulkley fluid.

H. A. Barnes, [9]and Zaman, Ali, & Sajid, [8] pointed out that the Cross model is complies with the viscosity shear rate of the human blood $Hb = 37\%$ and with experimental findings. Zaman et al. [8] noticed an increase in all flow characteristics except the resistance to flow through a porous-saturated stenotic artery. Rahman, Hossain, Mamun, & Akhter [10] concluded that at 75% constriction, the Cross model gave a better prediction than the Carreau and Newtonian model and that the flow velocity increases proportionately at the throat region with increase in the constriction or stenosis severity.

The present study considers the effect of tapering on streaming blood along a stenosed artery. Blood is treated using the Cross model constitutive equation to capture the physical properties of blood viscosity at both medium and high shear rate. The equations governing the flow are solved via the finite difference scheme. The results are compared with corresponding values of the Newtonian assumption.

2. **Problem Formulation**

2.1. Governing Equation

In this work, the streaming blood is modeled as an incompressible fluid. Blood flow through the artery is two-dimensional, axisymmetric and fully developed. Considering these assumptions, the governing equation in a cylindrical coordinate (r, θ, z) following the conservation of mass and momentum is presented as:

-continuity equation

$$\frac{\partial v}{\partial r} + \frac{v}{r} + \frac{\partial w}{\partial z} = 0, \tag{1}$$

-momentum equations

$$\frac{\partial w}{\partial t} + v\frac{\partial v}{\partial r} + w\frac{\partial w}{\partial z} = -\frac{1}{\rho}\frac{\partial p}{\partial z}\left[\frac{1}{r}\frac{\partial}{\partial r}(r\tau_{rz}) + \frac{\partial}{\partial z}(\tau_{zz})\right], \tag{2}$$

$$\frac{\partial v}{\partial t} + v\frac{\partial v}{\partial r} + w\frac{\partial v}{\partial z} = -\frac{1}{\rho}\frac{\partial p}{\partial z}\left[\frac{1}{r}\frac{\partial}{\partial r}(r\tau_{rr}) + \frac{\partial}{\partial z}(\tau_{rz})\right]. \tag{3}$$

the deviatoric stress tensor component takes the form

$$\tau_{rr} = -\mu\left(\dot{\gamma}\right)\left(2\frac{\partial v}{\partial r}\right), \quad \tau_{zz} = -\mu\left(\dot{\gamma}\right)\left(2\frac{\partial w}{\partial z}\right) \quad \tau_{zr} = \tau_{rz} = -\mu\left(\dot{\gamma}\right)\left(\frac{\partial v}{\partial z} + \frac{\partial w}{\partial r}\right),$$

The shear rate $\dot{\gamma}$ derived from the second invariant of the tensor is express as

$$\dot{\gamma} = \sqrt{2\left[\left(\frac{\partial v}{\partial r}\right)^2 + \left(\frac{v}{r}\right)^2 + \left(\frac{\partial w}{\partial z}\right)^2\right] + \left(\frac{\partial v}{\partial z} + \frac{\partial w}{\partial r}\right)^2} \tag{4}$$

The cross model was proposed by[11]

$$\mu\left(\dot{\gamma}\right)=\mu_{\infty}+\left(\mu_{0}-\mu_{\infty}\right)\left[1+\left(\left|\frac{\dot{\gamma}}{\gamma_{c}}\right|\right)^{m}\right]^{-1}.$$

For an axisymmetric flow, the shear stress and shear rate are described thus:

$$\tau_{zz}=-2\left[\mu_{\infty}+\left(\mu_{0}-\mu_{\infty}\right)\left\{1+\gamma_{c}^{2}\left[2\left(\left(\frac{\partial v}{\partial r}\right)^{2}+\left(\frac{v}{r}\right)^{2}+\left(\frac{\partial w}{\partial z}\right)^{2}\right)+\left(\frac{\partial v}{\partial z}+\frac{\partial w}{\partial r}\right)^{2}\right]^{n-1/2}\right\}^{-1}\right]\left(\frac{\partial w}{\partial z}\right), \tag{5}$$

$$\tau_{rz}=-\left[\mu_{\infty}+\left(\mu_{0}-\mu_{\infty}\right)\left\{1+\gamma_{c}^{2}\left[2\left(\left(\frac{\partial v}{\partial r}\right)^{2}+\left(\frac{v}{r}\right)^{2}+\left(\frac{\partial w}{\partial z}\right)^{2}\right)+\left(\frac{\partial v}{\partial z}+\frac{\partial w}{\partial r}\right)^{2}\right]^{n-1/2}\right\}^{-1}\right]\left(\frac{\partial w}{\partial r}+\frac{\partial v}{\partial z}\right), \tag{6}$$

$$\tau_{rr}=-2\left[\mu_{\infty}+\left(\mu_{0}-\mu_{\infty}\right)\left\{1+\gamma_{c}^{2}\left[2\left(\left(\frac{\partial v}{\partial r}\right)^{2}+\left(\frac{v}{r}\right)^{2}+\left(\frac{\partial w}{\partial z}\right)^{2}\right)+\left(\frac{\partial v}{\partial z}+\frac{\partial w}{\partial r}\right)^{2}\right]^{n-1/2}\right\}^{-1}\right]\left(\frac{\partial v}{\partial r}\right). \tag{7}$$

In Equation (1-7), v represents the radial velocity component while and w stand for the axial velocity components. ρ is the density of blood, the pressure is written as p and the stress tensor is denoted as τ. The dynamic viscosity of for non-Newtonian fluid is represented as $\mu\left(\dot{\gamma}\right)$. By applying simple approximations, other models like Power model (at intermediate shear rate) as well as the Sisko model can be deduced from the Cross model. The Cross model yields Newtonian values of μ_0 and μ_∞ that at very low and high shear rate. [12] described the pressure gradient as

$$-\frac{\partial p}{\partial z}=A_{0}+A_{1}\cos wt,\qquad t>0. \tag{8}$$

Here, the pressure gradient has an amplitude A_0 while the amplitude of the pulsatile component $w=2\pi f$, f is the hearts'pulse frequency.

The streaming blood and arterial wall are related considering these initial and boundary conditions.

$$v\left(r,z,t\right)=0\qquad \frac{\partial w\left(r,z,t\right)}{\partial r}=0\qquad \text{at}\qquad r=0, \tag{9}$$

$$w\left(r,z,t\right)=0\qquad v\left(r,z,t\right)=0\qquad \text{at}\qquad r=R, \tag{10}$$

$$w\left(r,z,t\right)=0\qquad v\left(r,z,t\right)=0\qquad \text{at}\qquad t=0. \tag{11}$$

2.2. Geometry of stenosis

Following [13] , the geometry of the arterial segment for the single stenosis for different tapering angles is mathematically expressed thus:

$$R(z,t)=\begin{cases}\left[(mz+a)-\dfrac{\tau_m sec\phi(z-d)}{\tau_m^2 sin\phi^2-\dfrac{l_0^2}{4}}\left[l_0-(z-d)\right]\right]a_1(t) & d<z<d+2z_0. \\ (mz+a).a_1(t) & otherwise\end{cases} \tag{12}$$

This time –variant geometry for multi- irregular stenosis can be obtained by multiplying the time independent radius $R(z)$ with the periodic function of time $a_1(t)$ describing the arterial wall is :

$$a_1(t)=1-bcos(\omega t+1)e^{(-b\omega t)}. \tag{13}$$

b is the amplitude and the whole segment of the artery is of finite length L. $R(z,t)$ and a represents the arterial radius for the tapered in the stenotic region and non-tapered artery in the non-stenotic region respectively The tapering angle is denoted by ϕ, d is the stenosis location and $\tau_m sec\phi$ stand for the critical length of stenosis in the tapered artery which appears at $z=d+\dfrac{l_0}{2}+\tau_m \sin\theta$ where the tapered vessel has a slope $m=\tan\phi$. ϕ determines the shape of the artery: the converging tapering ($\phi<0$), non-tapered artery($\phi=0$) and the diverging tapering ($\phi>0$).

3. Numerical procedure

3.1. The radial co-ordinate transformation

$$x=\frac{r}{R_{(z,t)}} \tag{14}$$

is employed to to immobilize the wall of the vessel in the newly transformed coordinate x, the continuity Equation 1 becomes

$$\frac{1}{R}\frac{\partial v}{\partial x}+\frac{v}{xR}+\frac{\partial w}{\partial z}-\frac{x}{R}\frac{\partial w}{\partial x}\frac{\partial R}{\partial z}=0. \tag{15}$$

The axial momentum in Equation 2 becomes

$$\frac{\partial w}{\partial t}=\left[\frac{x}{R}.\frac{\partial R}{\partial t}-\frac{v}{R}+w\frac{x}{R}.\frac{\partial R}{\partial z}\right]\frac{\partial w}{\partial x}-w\frac{\partial w}{\partial z}-\frac{1}{\rho}\frac{\partial p}{\partial z}-\frac{1}{\rho}\left[\frac{1}{xR}\tau_{xz}+\frac{1}{R}\frac{\partial \tau_{xz}}{\partial x}+\frac{\partial \tau_{zz}}{\partial z}-\frac{x}{R}\frac{\partial \tau_{zz}}{\partial x}\frac{\partial R}{\partial z}\right]. \tag{16}$$

The normal stress τ_{zz} in Equation 5 also becomes

$$\tau_{zz}=-2\left[\mu_\infty+(\mu_0-\mu_\infty)\left\{1+\gamma_c{}^2\left[2\left(\left(\frac{1}{R}.\frac{\partial v}{\partial r}\right)^2+\left(\frac{v}{xR}\right)^2+\left(\frac{\partial w}{\partial z}-\frac{x}{R}.\frac{\partial R}{\partial z}.\frac{\partial w}{\partial x}\right)^2\right)\right.\right.$$
$$\left.\left.+\left(\frac{\partial v}{\partial z}-\frac{x}{R}.\frac{\partial R}{\partial z}.\frac{\partial v}{\partial x}+\frac{1}{R}.\frac{\partial w}{\partial x}\right)^2\right\}^{\frac{n-1}{2}}\right]^{-1}\times\left(\frac{\partial w}{\partial z}-\frac{x}{R}\frac{\partial R}{\partial z}\frac{\partial w}{\partial x}\right). \tag{17}$$

Similarly, the shear stress in Equation 6

$$\tau_{xz}=-\left[\mu_\infty+(\mu_0-\mu_\infty)\left\{1+\gamma_c{}^2\left[2\left(\left(\frac{1}{R}.\frac{\partial v}{\partial r}\right)^2+\left(\frac{v}{xR}\right)^2+\left(\frac{\partial w}{\partial z}-\frac{x}{R}.\frac{\partial R}{\partial z}.\frac{\partial w}{\partial x}\right)^2\right)\right.\right.$$
$$\left.\left.+\left(\frac{\partial v}{\partial z}-\frac{x}{R}.\frac{\partial R}{\partial z}.\frac{\partial v}{\partial x}+\frac{1}{R}.\frac{\partial w}{\partial x}\right)^2\right\}^{\frac{n-1}{2}}\right]^{-1}\times\left(\frac{1}{R}\frac{\partial w}{\partial x}+\frac{\partial v}{\partial z}-\frac{x}{R}\frac{\partial R}{\partial z}\frac{\partial v}{\partial x}\right). \tag{18}$$

The boundary conditions (9-11) using the radial transformation becomes

$$v(x,z,t)=0, \qquad \frac{\partial w(x,z,t)}{\partial r}=0, \qquad \tau_{xz}=0 \quad \text{on} \quad x=0, \tag{19}$$

$$v(x,z,t)=\frac{\partial R}{\partial t}, \qquad w(x,z,t)=0 \quad \text{on} \quad x=1, \tag{20}$$

$$v(x,z,t)=0=w(x,z,t) \quad \text{at} \quad t=0. \tag{21}$$

3.2. The radial velocity component

The components $v(x,z,t)$ of the radial velocity is deduced by multiplying the transformed equation of continuity Equation 15 by xR then integrate with respect to x from limit 0 to limit x, i.e. from $x \to 0$.

$$\int_0^x x\frac{\partial v}{\partial x}dx+\int_0^x vdx+\int_0^x xR\frac{\partial w}{\partial z}dx-\int_0^x x^2\frac{\partial w}{\partial x}\frac{\partial R}{\partial z}dx=0,$$

$$xv-\int_0^x vdx+\int_0^x vdx+R\int_0^x x\frac{\partial w}{\partial z}dx-\frac{\partial R}{\partial z}\left[\left[x^2w\right]_0^x-\int_0^x 2xwdx\right]=0.$$

When simplified, it yields

$$xv+R\int_0^x x\frac{\partial w}{\partial z}dx-\frac{\partial R}{\partial z}x^2w+\frac{\partial R}{\partial z}\int_0^x 2xwdx=0,$$

$$v(x,z,t)=x\frac{\partial R}{\partial z}w-\frac{R}{x}\int_0^x x\frac{\partial w}{\partial z}dx-\frac{2}{x}\frac{\partial R}{\partial z}\int_0^x xwdx. \tag{22}$$

Applying the boundary condition in Equation 20 to Equation 22 gives

$$-\int_0^1 x\frac{\partial w}{\partial z}dx=\int_0^1 x\left[\frac{2}{R}\frac{\partial R}{\partial z}w+\frac{1}{R}\frac{\partial R}{\partial t}f(x)\right]dx. \tag{23}$$

Since the choice of $f(x)$ is arbitrary

$f(x)=4\left(1-x^2\right)$ which satisfies $\int_0^1 xf(x)dx=1,$

compare the left hand side of the arbitrary function to the right hand side of Equation 23

$$\frac{\partial w}{\partial z}=-\frac{2}{R}\frac{\partial R}{\partial z}w+\frac{4}{R}\left(x^2-1\right)\frac{\partial R}{\partial t}. \tag{24}$$

substituting Equation 24 into 22, we obtain

$$v(x,z,t)=x\frac{\partial R}{\partial z}w-\frac{R}{x}\int_0^x x\left[-\frac{2}{R}\frac{\partial R}{\partial z}w+\frac{4}{R}\left(x^2-1\right)\frac{\partial R}{\partial t}\right]dx-\frac{2}{x}\frac{\partial R}{\partial z}\int_0^x xwdx.$$

Simplification finally yields

$$v(x,z,t)=x\left[\frac{\partial R}{\partial z}w+\frac{\partial R}{\partial t}\left(2-x^2\right)\right]. \tag{25}$$

3.3. Discretization

The central difference approximation is employed in finite difference scheme to solve Equation 15 and 16 for all the first spatial derivatives which are:

$$\frac{\partial w}{\partial z}=\frac{(w)_{i+1,j}^{k}-(w)_{i-1,j}^{k}}{2\Delta z}=w_{fz}, \qquad \frac{\partial w}{\partial x}=\frac{(w)_{i,j+1}^{k}-(w)_{i,j-1}^{k}}{2\Delta x}=w_{fx}. \tag{26}$$

For the time derivative Equation 16, consider

$$\frac{\partial w}{\partial t}=\frac{(w)_{i,j}^{k}-(w)_{i,j}^{k}}{\Delta t}. \tag{27}$$

Also, the derivatives for v, τ_{zz} and τ_{xz} are

$$\frac{\partial v}{\partial x}=\frac{(v)_{i,j+1}^{k}-(v)_{i,j-1}^{k}}{2\Delta x}=v_{fx}, \quad \frac{\partial v}{\partial z}=\frac{(v)_{i+1,j}^{k}-(v)_{i-1,j}^{k}}{2\Delta z}=v_{fz}, \tag{28}$$

$$\frac{\partial \tau_{zz}}{\partial x}=\frac{(\tau_{zz})_{i,j+1}^{k}-(\tau_{zz})_{i,j-1}^{k}}{2\Delta x}=(\tau_{zz})_{fx}, \quad \frac{\partial(\tau_{zz})}{\partial z}=\frac{(\tau_{zz})_{i+1,j}^{k}-(\tau_{zz})_{i-1,j}^{k}}{2\Delta z}=(\tau_{zz})_{fz},$$

$$\frac{\partial \tau_{xz}}{\partial x}=\frac{(\tau_{xz})_{i,j+1}^{k}-(\tau_{xz})_{i,j-1}^{k}}{2\Delta x}=(\tau_{xz})_{fx}. \tag{29}$$

$w(x,z,t)$ is written as $w(x_j,z_i,t_k)$ for the purpose of discretization and hence denoted by $w_{i,j}^{k}$. Parameters are therefore defined as:

$x_j=(j-1)\Delta x; \qquad j=1,2,...N+1 \qquad$ where $\quad x_{N+1}=1.0$

$z_i=(i-1)\Delta z; \qquad i=1,2,...M+1,$

$t_k=(k-1)\Delta t; \qquad k=1,2,.....$

By substituting Equations 26 to 29 appropriately, the discretized form of Equations 16, 17 and 18 are

$$(w)_{i,j}^{k+1}=(w)_{i,j}^{k}+\Delta t\left[\frac{x_j}{R_i^k}\left(\frac{\partial R}{\partial t}\right)_i^k-\frac{v_{i,j}^k}{R_i^k}+(w)_{i,j}^{k}.\frac{x_j}{R_i^k}\left(\frac{\partial R}{\partial z}\right)_i^k\right]\left(\frac{\partial w}{\partial x}\right)_{i,j}^{k}-w_{i,j}^{k}.(w_{fz})_{i,j}^{k}$$
$$-\frac{1}{\rho}\left(\frac{\partial p}{\partial z}\right)_i^{k+1}-\frac{1}{\rho}\left[\frac{1}{x_jR_i^k}\tau_{xz}+\frac{1}{R_i^k}\left[(\tau_{xz})_{fx}\right]_{i,j}^{k}+\left[(\tau_{zz})_{fz}\right]_{i,j}^{k}-\frac{x_j}{R_i^k}\left[(\tau_{zz})_{x}\right]_{i,j}^{k}\left(\frac{\partial R}{\partial z}\right)_i^{k}\right], \tag{30}$$

$$\tau_{zz}=-2\left[\mu_\infty+(\mu_0-\mu_\infty)\left\{1+\gamma_c{}^2\left[2\left(\left(\frac{1}{R_i^k}.(v_{fz})_{i,j}^{k}\right)^2+\left(\frac{(v)_{i,j}^{k}}{x_jR_i^k}\right)^2+\left((w_{fz})_{i,j}^{k}-\frac{x_j}{R_i^k}.\left(\frac{\partial R}{\partial z}\right)_i^{k}.(w_{fx})_{i,j}^{k}\right)^2\right)\right.\right.$$
$$\left.\left.+\left((v_{fz})_{i,j}^{k}-\frac{x_j}{R_i^k}.\left(\frac{\partial R}{\partial z}\right)_i^{k}.(v_{fx})_{i,j}^{k}+\frac{1}{R_i^k}.(w_{fx})_{i,j}^{k}\right)^2\right\}^{\frac{n-1}{2}}\right]^{-1}\times\left((w_{fz})_{i,j}^{k}-\frac{x_j}{R_i^k}\left(\frac{\partial R}{\partial z}\right)_i^{k}(w_{fx})_{i,j}^{k}\right), \tag{31}$$

$$\tau_{xz}=-\left[\mu_\infty+(\mu_0-\mu_\infty)\left\{1+\gamma_c{}^2\left[2\left(\left(\frac{1}{R_i^k}.(v_{fz})_{i,j}^{k}\right)^2+\left(\frac{(v)_{i,j}^{k}}{x_jR_i^k}\right)^2+\left((w_{fz})_{i,j}^{k}-\frac{x_j}{R_i^k}.\left(\frac{\partial R}{\partial z}\right)_i^{k}.(w_{fx})_{i,j}^{k}\right)^2\right)\right.\right. \tag{32}$$

$$+\left(\left(v_{fz}\right)_{i,j}^{k}-\frac{x_j}{R_i^k}.\left(\frac{\partial R}{\partial z}\right)_i^k.\left(v_{fx}\right)_{i,j}^{k}+\frac{1}{R_i^k}.\left(w_{fx}\right)_{i,j}^{k}\right)^2\Bigg\}^{\frac{n-1}{2}}\Bigg]^{-1}\times\left(\left(v_{fz}\right)_{i,j}^{k}-\frac{x_j}{R_i^k}\left(\frac{\partial R}{\partial z}\right)_i^k.\left(v_{fx}\right)_{i,j}^{k}+\frac{1}{R_i^k}\left(w_{fx}\right)_{i,j}^{k}\right).$$

The discretised boundary conditions Equation 19 to 21 is of the form

$$\left(v\right)_{i,j}^{k}=0,\qquad \left(w\right)_{i,1}^{k}=\left(w\right)_{i,2}^{k}\qquad \left(\tau_{xz}\right)_{i,1}^{k}=0, \tag{33}$$

$$\left(w\right)_{i,N+1}=0,\quad \left(v\right)_{i,N+1}^{k}=\left(\frac{\partial R}{\partial t}\right)_i^k, \tag{34}$$

and

$$\left(v\right)_{i,j}^{1}=0,\qquad \left(w\right)_{i,j}^{1}=0. \tag{35}$$

To calculate the component, w, of the axial velocity, Equations 31 to 32 is solved considering the boundary conditions in Equations 33 to 35. The radial velocity component Equation 25 is discretized as

$$\left(v\right)_{i,j}^{k+1}=x_j\left[\left(\frac{\partial R}{\partial z}\right)_i^k w_{i,j}^{k+1}+\left(\frac{\partial R}{\partial t}\right)_i^k\left(2-x_j^{\,2}\right)\right]. \tag{36}$$

With the value of the axial component, Equation 36 can be used to obtain the radial velocity. The results obtained can be substituted into the Equations below to deduce the volumetric flow rate $\left(Q\right)$, flow resistance $\left(\Omega\right)$, as well as the wall shear stress $\left(\tau_w\right)$.

$$Q_i^k=2\pi\left(R_i^k\right)^2\int_0^1 x\left(w\right)_{i,j}^{k}\,dx_j, \tag{37}$$

$$\Omega_i^k=\frac{\left|L\left(\partial p/\partial z\right)^k\right|}{Q_i^k}, \tag{38}$$

$$\left(\tau_w\right)_i^k=\mu\left[\frac{1}{R_i^k}.\left(w_{fx}\right)_{i,j}^{k}+\left(v_{fz}\right)_{i,j}^{k}-\frac{x_j}{R_i^k}\left(v_{fx}\right)_{i,j}^{k}.\frac{\partial R^{\,k}}{\partial z_{\,i}}\right]_{x=1}\times\cos\left(\tan^{-1}\left(\frac{\partial R}{\partial z}\right)_i^k\right). \tag{39}$$

4. Simulation results and discussion

In this section, the numerical results are presented after a steady state is achieved following he parameter values [6], [14];
$a=0.08cm,\ L=5.0cm,\ l_o=1.6cm\,,\ d=2.0cm,\ b=0.1,\ m=0.1735P,\quad \mu=0.035P,\ n=0.639,\ \rho=1.06gcm^{-3},\ f_p=1.2Hz, A_0=10gcm^{-2}s^{-2}, A_1=0.2\,A_0,\ \Delta x=0.025,\ \Delta z=0.1,$ and $\tau_m=0.4a$. With time step $\Delta t=0.00001$, convergence is attained with an accuracy of order$\sim 10^{-7}$. Solutions are computed for this computational domain using the grid 50×40 for z and x respectively.

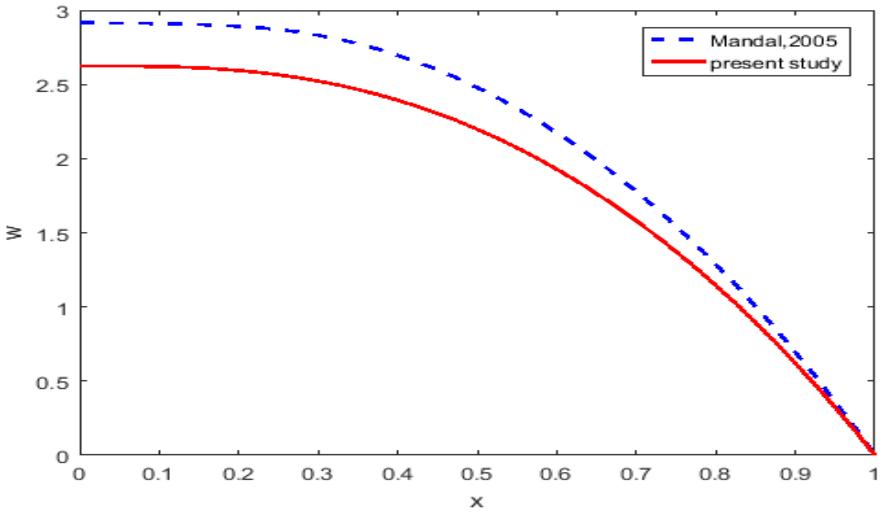

Figure 1. Axial velocity profile at $z = 28mm$ for $t = 0.45s$

$(\tau_m = 0.4a, d = 20mm, l_0 = 16mm, \phi = -0.1)$

Figure 1 shows a close agreement with the prediction of [13] with a slight variation which may be due to the change in model used. The graph illustrates the profile of the axial velocity for blood flow using the Cross (non-Newtonian) model at location $z = 28mm$ in the stenotic area of tapered artery for time $t = 0.45s$ with the dimensionless radial position x (given in the second boundary condition). It could be observed that the curve decrease from its maximum point and eventually drops to zero at the wall surface. The curve has a parabolic shape at $(\phi = -0.1^0)$ when considered under a stenotic condition. This observation agrees with [13], [15] who compared the velocity profiles of converging and diverging arteries and concluded that axial velocities reduces with vessel tapering.

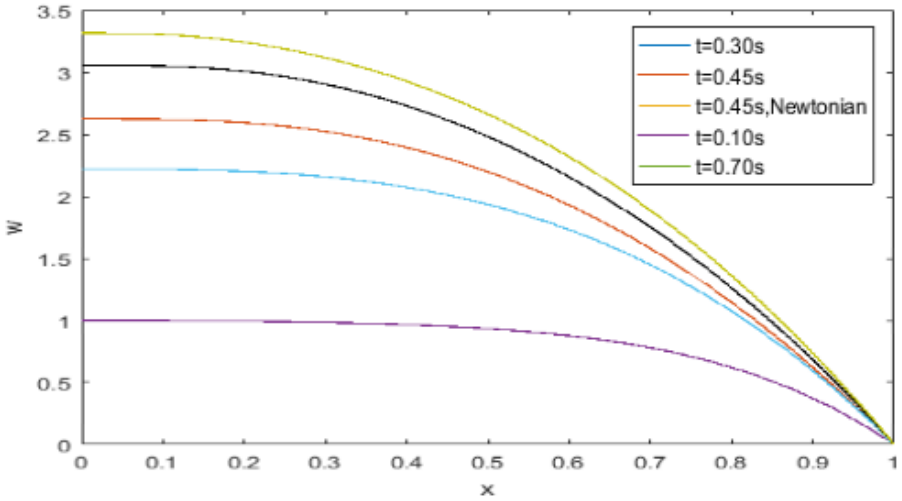

Figure 2. Radial velocity profile at $z = 28mm$ for $t = 0.45s$

$(\tau_m = 0.4a, d = 20mm, l_0 = 16mm, \phi = -0.1\,)$

Figure 2 illustrates the variation in the profile of the axial velocity considering the critical location ($z = 28mm$) at different times within a single cardiac cycle. A downward bend towards the origin was experienced with proportionate increase on time. i.e. from 0.1s to 0.45s. On the other side, the curve was found to shift further from the origin at time t=0.7s. According, to [16], this experience in the axial velocity profile is elicited by the pulsatile pressure gradient as the heart pumps. As expected physiologically, the decline in the axial velocity in the systolic phase takes place at an approximate time as the rate of increase in the diastolic phase.

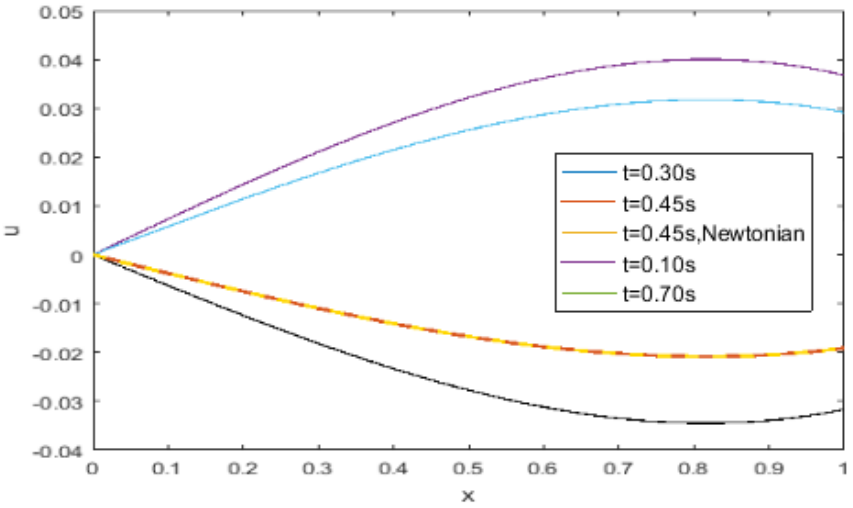

Figure 3. Radial velocity profile at $z = 28mm$ for $t = 0.45s$

$(\tau_m = 0.4a, d = 20mm, l_0 = 16mm)$

Figure 3 describes the radial motion in the wall of the artery measure at the same critical location for a cardiac cycle. At the systolic stage (from 0.1s to 0.3s), the curves in the radial velocity profile are positive but the reverse is the case during the diastolic stage (0.45s to 0.7s) where a back flow was experienced with a negative radial velocity profile. It can also be observed that the Newtonian behavior of the streaming blood in the radial velocity is of lesser effect as compared to that of the axial velocity.

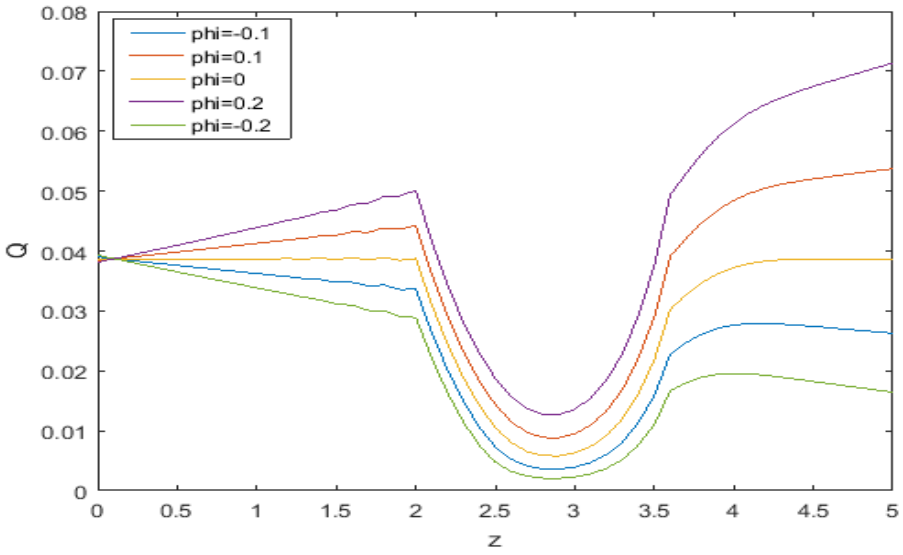

Figure 4. Radial velocity profile at $z = 28mm$ for $t = 0.45s$

$(\tau_m = 0.4a, d = 20mm, l_0 = 16mm)$

Figure 4 describes the effect of tapering on blood flow rate within a single cardiac cycle. The tapering angles ranges from -0.1 to 0.2. The figure shows that the values volumetric flow rate for the diverging tapering are higher than those of the converging tapering as well as the non-tapered artery.

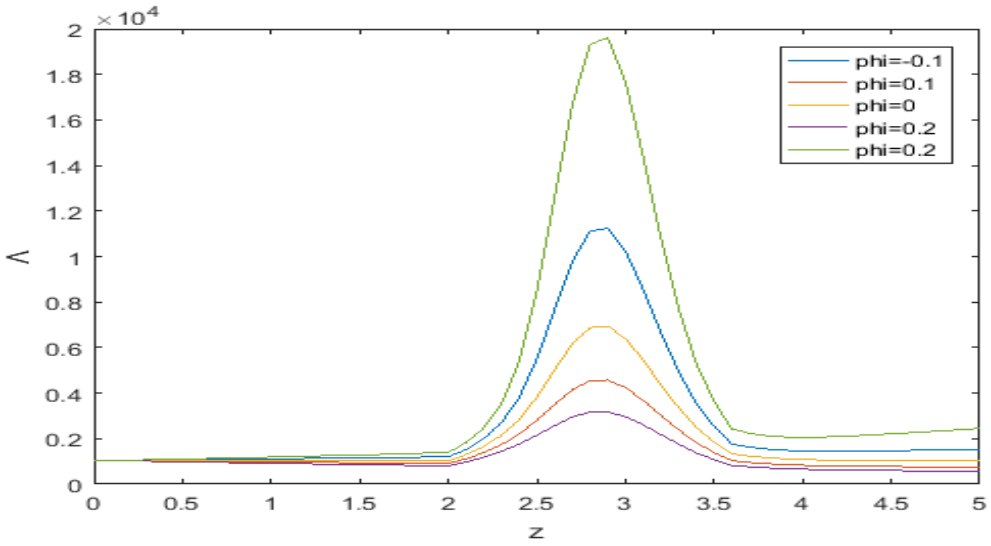

Figure 5. Radial velocity profile at $z = 28mm$ for $t = 0.45s$

$(\tau_m = 0.4a, d = 20mm, l_0 = 16mm)$

From figure 5, The values of the resistance to flow in converging tapering are higher than those of the diverging tapering as well as the non-tapered artery. This experience is the direct reversal of the volumetric flow rate. The effect of resistance on converging tapered arteries appears to be more

obvious than it does on the diverging tapered arteries. Hence, since the resistance to flow is less, blood flows more freely in the diverging vessels.

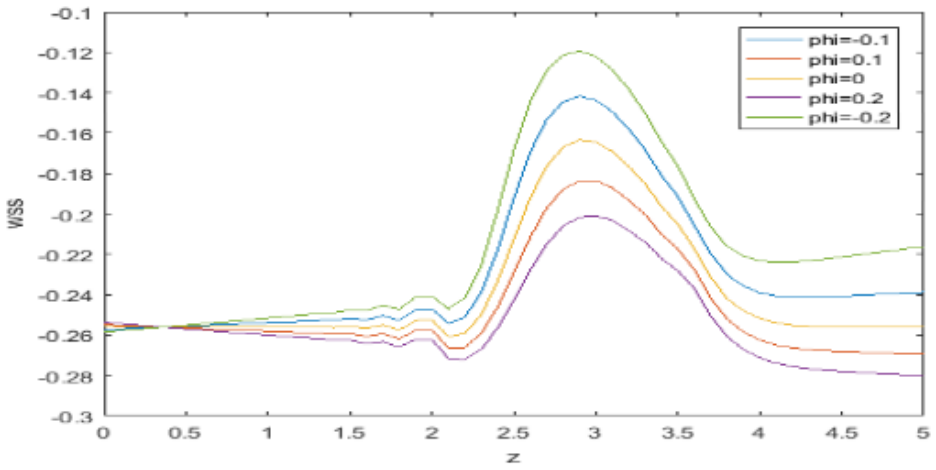

Figure 6. Radial velocity profile at $z = 28mm$ for $t = 0.45s$

$(\tau_m = 0.4a, d = 20mm, l_0 = 16mm)$

Across the arterial wall, the flow properties are greatly influenced by the wall shear stress. Figure 6 depicts the variation that exist at the arterial boundary for the shear stress at different tapering angles. Like the resistance to flow, the values of converging tapering for the wall shear stress were higher than those of the diverging artery and the non-tapering arteries. The variation, appears to be similar with the flow resistance.

5. Conclusion

The theoretical model of pulsatile flow of blood in a tapered artery having a single stenosis using the Cross model are presented. The main focus of this work is to evaluate the effect of vessel tapering on flowing blood. The tapering angles of artery were classified into three: converging tapering ($\phi < 0$), non-tapered ($\phi = 0$) and diverging tapering ($\phi > 0$)in the presence of stenosis. It was observed that as the tapering angle increases the flow rate and the axial velocity increases proportionately while the radial velocity, flow resistance and the wall shear stress decreases.

References

[1] Changdar S and De S 2016 *Arab. J. Math.* **5(1)** 51–61
[2] Reddy J V R, Srikanth D and Mandal P K 2017 *Int. J. Appl. Comput. Math.* **3** S1 1261–1287
[3] Zaman A, Ali N, Sajid M and Hayat T 2015 *AIP Adv.*5**(3)** 037129
[4] Rabby M G, Razzak A and Molla M M 2013 in Procedia Eng. **56** 25–231
[5] Rabby M G, Shupti S P and Molla M M 2014 *J. Fluids* **2014** 1–13
[6] Shupti S P, Molla M M and Mia M 2017 *Front. Mech. Eng.* 3 1–15
[7] Priyadharshini S and Ponalagusamy R 2015 *Appl. Bionics Biomech.* **2015** 1-12
[8] Zaman A, Ali N and Sajid M 2017 *Math. Comput. Simul.* **134** 1–16
[9] Barnes H A, Barnes Hutton J F K and Walters K 1989 *An Introduction to Rheology, Elsevier Science Publishers, Amsterdam*
[10] Rahman M M, Hossain M A, Mamun K and Akhter M N 2018 *AIP Conf. Proc.*1851
[11] Cross M M 2965 *J. Colloid Sci.* **20(5)** 417–437

[12] Burton A C 1966 *Physiology and biophysics of the circulation : an introductory text TT -, 2d ed. Chicago, Ill. : Year Book Medical Publishers*
[13] Mandal P K 2005 *Int. J. Non. Linear. Mech.* **40(1)** 151–164
[14] Vlachopoulos W W N 1974 *Charalambos, Michael O'Rourke, McDonald's blood flow in arteries: theoretical, experimental and clinical principles* **9(6)**
[15] Ismail Z, Abdullah I, Mustapha N and Amin N 2008 *Appl. Math. Comput.***195(2)** 669–680
[16] Chakravarty S, Mandal P K and Sarifuddin 2005 *Int. J. Non. Linear. Mech.* **40(10)** 1268–1281